agriculture

MDPI

Article

Vortex Cleaning Device for Rice Harvester: Design and Bench Test

Weijian Liu [1], Shan Zeng [2] and Xuegeng Chen [1,*]

[1] Key Laboratory of Modern Agricultural Equipment and Technology, Ministry of Education, Jiangsu University, Zhenjiang 212013, China; 1000005920@ujs.edu.cn
[2] College of Engineering, South China Agricultural University, Guangzhou 510642, China; shanzeng@scau.edu.cn
* Correspondence: chenxg130@sina.com; Tel.: +86-0511-80967736

Abstract: To solve the problem of increased grain impurity rate and grain loss rate caused by clogging of sieve holes during the cleaning process of ratooning rice, a spiral step cleaning device was designed, which disturbed the flow field at the sieve holes through vortex in the slot and disrupted the force balance of the blockages at the sieve holes. The device mainly includes a cleaning separation core and a cleaning separation core shell. Firstly, the main parameters of the cleaning separation core were determined, and the critical shear airflow velocity was obtained through theoretical analysis. Through energy loss analysis, the fan wind speed was determined to be 11.5 m/s. Secondly, the CFD-DEM coupling method was used to analyze the flow patterns inside the slot and the movement patterns of blockages on the sieve surface, confirming the effectiveness of vortex guided blockage removal. Finally, a prototype was designed and built for testing, and the results showed that when the wind speed of the fan was 11.5 m/s, the grain impurity rate was 1.35%, the grain loss rate was 2.13%, and the average sieve blockage rate was ≤0.1%. All indicators were better than traditional cleaning devices and could meet the cleaning requirements. During the continuous operation of the spiral step cleaning device, performance indicators such as sieve hole blockage rate remained basically unchanged.

Keywords: ratooning rice; vortex blockage removal; spiral step cleaning; CFD-DEM coupling; test

check for updates

Citation: Liu, W.; Zeng, S.; Chen, X. Vortex Cleaning Device for Rice Harvester: Design and Bench Test. *Agriculture* **2024**, *14*, 866. https://doi.org/10.3390/agriculture14060866

Academic Editor: Bruno Bernardi

Received: 10 April 2024
Revised: 20 May 2024
Accepted: 29 May 2024
Published: 30 May 2024

Copyright: © 2024 by the authors. Licensee MDPI, Basel, Switzerland. This article is an open access article distributed under the terms and conditions of the Creative Commons Attribution (CC BY) license (https://creativecommons.org/licenses/by/4.0/).

1. Introduction

The rice growing area in China is about 30 million hectares, with an annual output of more than 210 million tons [1,2]. Ratooning rice has the advantages of planting once and harvesting twice, making full use of light and temperature resources, increasing grain production and income, and good rice quality, etc., which has been rapidly promoted in recent years in suitable areas in the middle and lower reaches of the Yangtze River [3,4]. Cleaning is a key link in the harvesting operation of the ratooning rice [5]. At present, the cleaning system is mainly divided into three types: airflow type, sieve type and combined air flow sieve type [6,7], and the performance indicators include impurity rate, loss rate, separation efficiency [8], etc. Due to the high moisture content and strong adhesion of ratooning rice, simple airflow and vibration cannot separate ratooning rice from impurities. When using traditional cleaning devices to clean ratooning rice, sieve clogging often occurs, which increases the loss rate and impurity rate, seriously affecting the yield of ratooning rice.

Scholars at home and abroad have conducted extensive research on the problem of sieve clogging in traditional agricultural equipment. ASTROM [9] designed a rotating probability sieve and determined through experiments that the opening rate of the rotating probability sieve is more stable than that of the linear vibrating sieve; Chen Shuren et al. [10] proposed to reduce the accumulation and blockage of materials on the screen surface by increasing the amplitude of the front end of the screen surface and decreasing the amplitude

of the back end of the screen surface; Yang Huimin et al. [11] proposed using elastic sieve surfaces instead of metal sieve surfaces to avoid clogging of sieve holes; Li Yaoming et al. [12] proposed that the non smooth sieve surface has the effect of reducing adhesion and detachment in the cleaning process of rapeseed, in response to the problems of adhesion and blockage in the cleaning sieve. However, the above methods cannot fundamentally solve the problem of sieve clogging. When cleaning crops with high moisture content and strong adhesion, sieve clogging still occurs.

In response to the problem of sieve blockage in traditional cleaning equipment for cleaning ratooning rice, this article designs a spiral step cleaning device. As a bionic cleaning structure, spiral step cleaning is a modified cross-flow cleaning process that can prevent clogging and further enhance the cleaning efficiency through the circulating vortex in cleaning device slots [13,14]. It is not feasible to visualize the vortices located in the slots between the cleaning device's skeletons using fibreoptic endoscopy, thus numerical simulation is an effective way. For simulating gas-solid two-phase flow in challenging 3D recirculation [15], CFD-DEM coupling based on Hertz contact theory and Newton's law of motion is a promising option [16,17]. In this paper, the effect of the vortex state inside spiral step cleaning devices on blockage deposits on sieve is studied using a numerical simulation of gas-solid two-phase flow. And the effectiveness of the model was verified through bench tests, providing a basis and reference for the design of the cleaning system of the ratooning rice harvester. If calculated based on rice yield of 0.75 kg/m^2, using a spiral step cleaning device can recover a loss of 0.12 yuan/m^2. The planting area of ratooning rice in China is 9.9×10^9 m^2, which will recover a loss of 1.2 billion yuan. The development of a spiral step cleaning device has high economic value.

The primary goal of this study was to provide a clearing device and a method for reducing grain loss rate and grain impurity rate in the cleaning of ratooning rice. The detailed objectives were: (1) design a spiral step cleaning device; (2) establish a mathematical model and carry out a coupling simulation of the discrete element method (DEM) and computational fluid dynamics (CFD) for studying the the flow field inside the device and the motion law of blockage on the surface of the sieve under the action of vortices; (3) carry out a bench test to verify the effectiveness of the spiral step cleaning device.

2. Structure and Working Principle

2.1. Structure of the Cleaning Device

The spiral step cleaning device mainly consists of a cleaning chamber shell and an internal cleaning separation core, and a three-dimensional model of the device is drawn using CATIAV5R20 (Dassault Systems, Vélizy-Villacoublay, France), as shown in Figure 1.

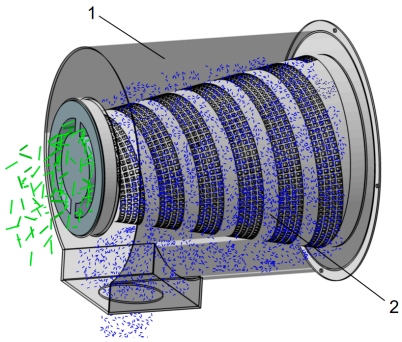

Figure 1. The structure of the spiral step cleaning device. (1) Cleaning and separation core shell (2) Cleaning separation core. Blue represents the grains of ratooning rice, while green represents impurities.

The cleaning separation core is composed of a double helix skeleton with a gradually decreasing diameter and a sieve (Figure 2a). The gaps of the sieve allow the ratooning rice to pass through, leaving impurities on the sieve. The remaining impurities on the sieve can only be discharged through the impurity outlet at the tail of the cleaning separation core.

In order to facilitate the expression of particle distribution positions, adjacent skeletons are named and the sieves between adjacent spiral skeletons were divided into front sieve (Area A), overflow sieve (Area B) and rear sieve (Area C), as shown in Figure 2b. The cleaning slots were numbered along the direction of air flow movement, as shown in Figure 2c.

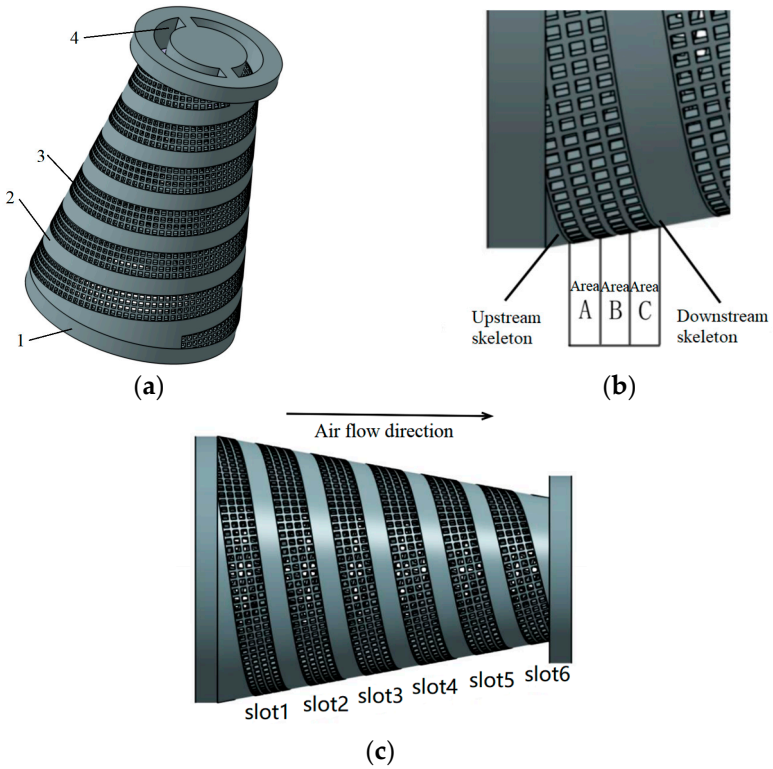

Figure 2. Structure diagram of cleaning separation core. (1) Mixture inlet (2) Spiral skeleton (3) Sieve (4) Impurity outlet. (**a**) Cleaning separation core axonometric drawing; (**b**) Sieve diagram; (**c**) Side view of cleaning separation core. Area A: front sieve; Area B: overflow sieve; Area C: rear sieve.

2.2. Determination of Main Parameters for Cleaning Separation Core

The main parameters that affect the effectiveness of vortex blockage removal are: ratio of inlet area to cleaning area F, proportion coefficient G [18], slot angle α and cone angle γ, as shown in Figure 3.

$$G = \frac{w}{h} \tag{1}$$

$$F = \frac{S_m}{S_{in}} \tag{2}$$

where h is the skeleton thickness, mm; w is the slot height, mm; S_{in} is the cleaning separation core sieve area, mm^2; S_m is the cleaning separation core inlet area, mm^2.

According to the proportion coefficient G, the cleaning separation core skeleton can be divided into type K (G > 4) and type D (G < 3~4) [19]. In the cleaning process, the D-type cleaning separation core skeleton can form a circulating vortex that is fully in contact with the cleaning slot sieve, thereby improving the cleaning effect and reducing the blockage of the sieve [20–22]. Based on the above analysis and the actual installation space of the cleaning system, the parameters of the cleaning separation core are shown in Table 1.

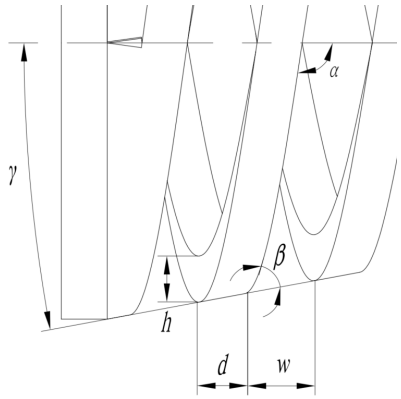

Figure 3. Main parameters of clean separation core. NOTE: γ represents the cone angle, ° represents the unit of angle; h represents the thickness of the skeleton, mm; d represents the height of the skeleton, mm; w represents the height of the slot, mm; α represents the angle of the slot, °; β represents the inclination angle of the skeleton, °.

Table 1. Cleaning separation core parameters.

Parameter	Value
Total length/mm	680
Mixture inlet diameter/mm	480
Impurity outlet diameter/mm	350
Sieve aperture/mm	15
Skeleton thickness h/mm	30
Skeleton height d/mm	30
Slot height w/mm	60
Slot angle α/°	98
Skeleton inclination angle β/°	64.1
Cone angle γ/°	10.5

2.3. Working Principle

The cross-flow area of the cleaning separation core decreases gradually along the direction of mixed flow movement. During the cleaning process, the mixed flow can evenly enter each cleaning slot. After passing through the spiral skeleton, the sudden increase in flow area causes the airflow to rotate and form vortices in the slot. Under the action of vortices, the mixed flow comes into full contact with the sieve, and the ratooning rice is screened out, leaving impurities on the surface of the sieve. Subsequently, the impurities on the surface of the sieve are blown into the inner corner of the upstream skeleton under the action of shear flow. Shear flow interferes with the movement of impurities on the surface of the sieve, disrupting their force balance and achieving cleaning of the sieve holes.

3. Mathematical Methods

Obtained mathematical formulas for CFD-DEM method from literature [23]. The CFD-DEM coupling method consists of equations for controlling particle rotational motion and translation, Navier Stokes equations, and continuity equations for mass conservation [24]. Due to the bridging mechanism between particles on the screen of the spiral step cleaning device, an adhesion model based on Johnson Kendall Roberts (JKR) theory was used [25]. In CFD, the airflow in the spiral step cleaning device is considered viscous. The wall surface is rough, and the surface tension is ignored. Simplify the shell to the surface and simplify the sieve to the interior wall, which is configured as a porous jumping boundary. The formula for the pressure drop ΔP_m on the grid is as follows:

$$\Delta P_m = -\left(\frac{\mu}{\alpha_p} v + C_2 \frac{1}{2} \rho v^2\right) \Delta m \tag{3}$$

Grid division of the cleaning device, as shown in Figure 4a. Three different specifications of grid systems were used to test the convergence of the grid, as shown in Table 2. When the number of grids reaches 6.6×10^6, as the grid size decreases, the simulated pressure drop on the step cleaning device will converge. Therefore, this computational model has grid independence.

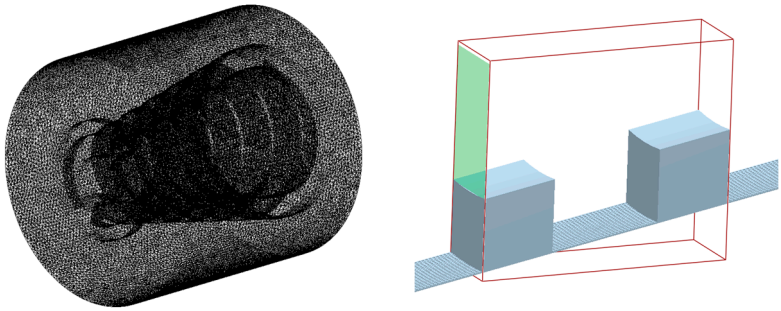

(**a**) (**b**)

Figure 4. Grid model of spiral step cleaning device. (**a**) Grid partitioning. (**b**) Calculation area.

Table 2. Grid convergence test.

Grid Number/10^6	Pressure Drop across Filter ΔP_f/Pa	Relative Deviation/%
11.3	1181	/
6.6	1154	2
3.4	1035	12

Due to the presence of reflux and eddy currents inside the spiral step cleaning device, the standard *k*-ε model was used in the simulation. The outlet was set as a pressure outlet, and the boundary conditions are analyzed using the standard wall function method.

In DEM, the movement and distribution of particles in the cleaning slot are key issues in simulating the removal of blockages. The barrier effect of the spiral skeleton results in minimal influence between slots [26]. Therefore, it is only necessary to study the influence of the flow state inside one of the cleaning slots on the mixture in the cleaning slot. In order to simplify the mesh in the DEM geometric model, the geometric structure of square hole mesh was adopted, as shown in Figure 4b. The green area represents the location of the generated particles, while the red boundary represents the computational domain.

The fluid computational domain coupled with the grid model of DEM is called the coupling domain, while the rest of the fluid computational domain is called the decoupling domain [27]. The flow field data applies force to particles in the DEM, and the force acting on the fluid is determined by the particle position in the DEM. The numerical solution strategy for CFD-DEM coupling is shown in Figure 5.

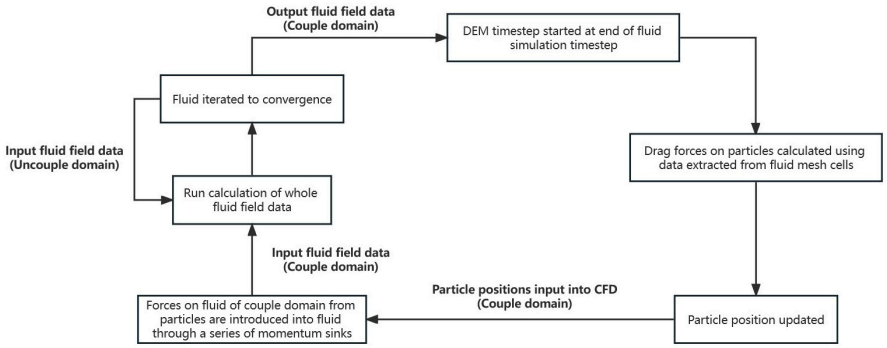

Figure 5. Numerical solution strategy for CFD-DEM coupling.

4. Design of Key Components and Determination of Parameters

4.1. Force Analysis of Blockages

The blockage is mainly composed of ratooning rice and impurities. Through experiments, the suspension speed of ratooning rice grains is approximately 6–8 m/s, and the suspension speed of broken stems (impurities) is 2.5–3.5 m/s. The blockage at the sieve holes is subjected to gravity mg, shear force F_{t1} provided by the vortex, penetration force F_{t2} provided by the vortex, support force F_N provided by the sieve mesh, and friction force f. The force acting on the blockage at the sieve holes is shown in Figure 6.

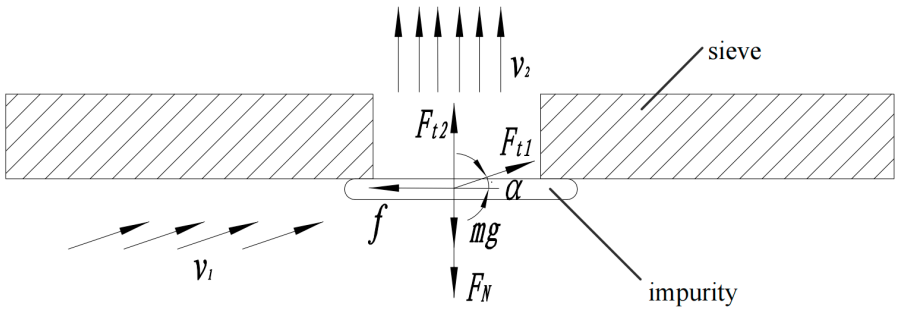

Figure 6. Force analysis of blockages.

The shear force F_{t1} acting on the blockage is:

$$F_{t1} = \frac{1}{2} C A \rho_s v_1 \tag{4}$$

where A is the material windward area, m^2; C is the material resistance coefficient, $C = 0.33$; ρs is the material density, kg/m^3; v_1 is the shear flow velocity, $v_1 = 3$ m/s. According to previous research, $\alpha = 9°$.

The penetration force F_{t2} provided by the vortex on the blockage is:

$$F_{t2} = \frac{1}{2} C A \rho_s v_2 \tag{5}$$

where v_2 is the penetrating flow velocity, m/s.

When the sieve is blocked, at the moment when the blockage separates from the sieve, $F_N = 0$ N, the force acting on the blockage is:

$$F_{t\ 2} + F_{t1} \sin \alpha = mg \tag{6}$$

where m is the mass of the blockage, kg; g is the gravitational acceleration, 9.81 m/s^2.

To break the force balance of the blockage at the sieve hole and achieve vortex cleaning, the sum of the penetration force and shear force provided by the vortex in the positive y-axis direction should be less than the gravity of the mixture. The relationship formula is:

$$F_{t\ 2} + F_{t1} \sin \alpha < mg \tag{7}$$

The relationship formula for penetrating flow velocity v_2 is:

$$v_2 < \frac{2mg}{CA\rho_s} - v_1 \sin \alpha \tag{8}$$

After testing, the average mass of blockage in each sieve hole is 4.5 g, with an average density of 90.5 kg/m^3, the average windward area of the blockage is 5.57×10^{-4} m^2. The penetrating flow velocity $v_2 < 4.96$ m/s.

4.2. Determination of Fan wind Speed

To determine the wind speed of the fan, the energy loss in the cleaning device is analyzed. The airflow is generated by the fan and fed into the pipeline to reach the inlet of the cleaning separation core. The energy loss includes both along the way loss and local loss [28,29], and the relationship formula is:

$$\begin{cases} h_{f1} = \lambda \frac{L}{d} \frac{v^2}{2g} \\ h_{f2} = \xi \frac{v^2}{2g} \end{cases} \tag{9}$$

where h_{f1} and h_{f2} are the loss along the path and local loss, m; L is the length of the conveying pipe, m; d is the diameter of conveying pipe, m; v is the airflow velocity, m/s; λ is the loss coefficient along the way; ζ is the local loss coefficient, ζ = 1.2.

Considering the energy loss of airflow during the flow process, the Bernoulli equation from the fan outlet to the cleaning separation core inlet along the flow direction is:

$$\frac{p_1}{\rho g} + z_1 + \frac{\delta_1 v_3{}^2}{2g} = \frac{p_2}{\rho g} + z_2 + \frac{\delta_2 v_4{}^2}{2g} + \sum h_f \tag{10}$$

where p_1 and p_2 are the static pressure at the outlet of the fan and the inlet of the cleaning separation core, respectively, N/m^2; δ_1 and δ_2 are the kinetic energy correction coefficients for the fan outlet section and the cleaning separation core inlet section, respectively; z_1 and z_2 are the water heads at the outlet of the fan and the inlet of the cleaning separation core, respectively, m; ρ is the air density, kg/m^3; v_3 and v_4 are the airflow velocity at the outlet of the fan and the inlet of the cleaning separation core, m/s.

Using Fluent (Fluent (19.0, ANSYS Inc., Canonsburg, PA, USA)) software, set different fan wind speeds and record the maximum penetrating flow velocity in each slot. Use Origin (Origin (2020, OriginLab Inc., Northampton, MA, USA)) software to perform curve fitting on the obtained data [30–32]. Based on the imported data, set the fitting equation to be a univariate linear equation y = ax + b. The fitting curve equation is:

$$y = 1.725x + 1.7714 \tag{11}$$

Substitute the maximum penetrating flow velocity into Equation (11), and based on the Bernoulli equation, calculate the wind speed of the fan as 11.5 m/s. Through simulation verification, it can be concluded that when the wind speed of the fan is 11.5 m/s, the average penetrating flow velocity inside the device is 4.305 m/s, with a maximum value of 4.89 m/s, meeting the requirements for sieve cleaning, simulation process is shown in Figure 7.

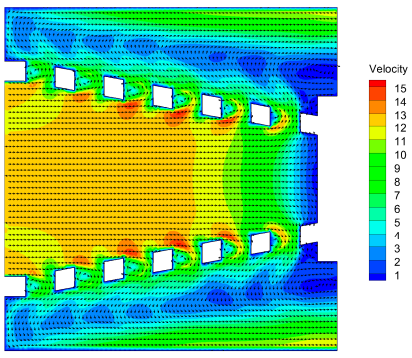

Figure 7. Simulation analysis of flow velocity inside the cleaning device. The white squares in the figure represent the spiral skeleton of the cleaning device.

4.3. Slot Vortex

Due to the fact that vorticity not only includes the rotation of the fluid, but also the deformation, shear, and compression of fluid micro clusters, the size and center point of vortices cannot be determined solely based on vorticity. For example, Figure 8a uses the Ω vorticity discrimination method [22], where the rotation of the airflow generates a higher vorticity, resulting in it being regarded as a vortex by the discrimination method. However, the upstream wall shear flow is ignored due to its smaller vorticity. Using the streamline method to identify vortices, the closed streamline with the largest area is considered as the boundary of the vortex, and the flow velocity and rotational speed of the vortex are calculated based on its circulation. The vortex core is located at the zero point of the flow velocity at the center of the vortex, as shown in Figure 8b and Table 2.

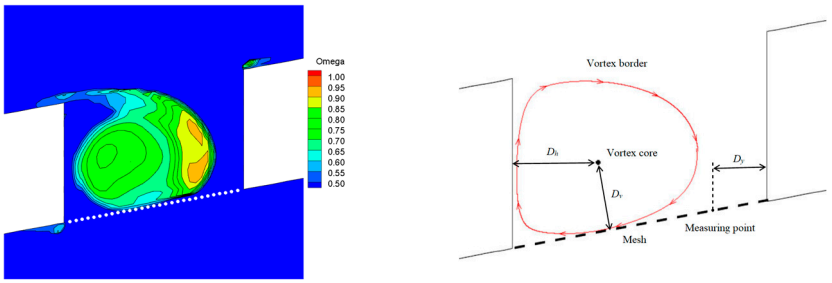

(**a**) (**b**)

Figure 8. Definition and identification of vortex in slot 5. (**a**) Omega vortex identification method (**b**) vortex identification method based on streamlines. **Note:** In the core location, the first coordinates D_h indicates the minimum distance between the vortex core and the upstream skeleton and the second coordinates D_v indicates the minimum distance between the vortex core and the sieve (Figure 6b).

Table 3 indicates that the vortex core gradually moves toward the upstream skeleton and sieve, and its area and diameter decrease slowly from slot 1 to 6. The position and size of the vortex are influenced by shear flow. From slots 2 to 6, the velocity first increases and then decreases, reaching its maximum value in slot 5. The rotational speed also exhibit the same trend.

Table 3. Parameters of vortex.

Slot Number	1	2	3	4	5	6
Core location/(mm)	(23.3, 16.6)	(21.7, 16.3)	(21.3, 16.7)	(20.3, 16.1)	(20.8, 16.2)	(20.2, 15.7)
Area/(mm^2)	1564	1481	1399	1367	1303	1276
Circumference/(mm)	143.2	140.3	139.6	138.8	137.9	137.2
Velocity/($cm \cdot s^{-1}$)	61.89	55.67	58.36	64.29	68.51	66.18
Rotational speed/($n \cdot min^{-1}$)	1277	1181	1269	1418	1483	1439

5. Particle Movement and Distribution in the Slots

5.1. Particle Modeling and Simulation Parameter Setting

For the ratooning rice used in the experiments, the water content was 16–30% and the range of density was 983–1369 kg/m^3 (approximately they were in an ellipsoid shape) [33,34]. The approximated geometric shape of a rice grain was as follows: the length of 5.00–8.35 mm, the width of 1.91–3.25 mm, the height of 2.0–3.0 mm, and the average length of 7.21 mm. A model of ratooning rice and impurities was established using a combination of multiple spheres in EDEM [35,36]. The simulation parameters were set by consulting literature, as shown in Table 4.

Table 4. Characteristic parameters of ratooning rice and impurities.

Parameter	Ratooning Rice	Impurities
Semi-axes (L × B × H)/mm	7.21 × 2.15 × 2.21	32.12 × 4.15 × 4.21
Poisson's ratio	0.25	0.4
Elastic modulus/Pa	3.75×10^8	1.15×10^6
Density/kg·m^{-3}	1330	243
Recovery coefficient among ratooning rice grains/impurities	0.6	0.4
Static friction factor among ratooning rice grains/impurities	0.3	0.24
Rolling friction factor among ratooning rice grains/impurities	0.01	0.05

5.2. Flow State Analysis

Conduct simulation experiments, set the wind speed of the fan to 11.5 m/s, and analyze the airflow velocity in six slots, as shown in Figure 9.

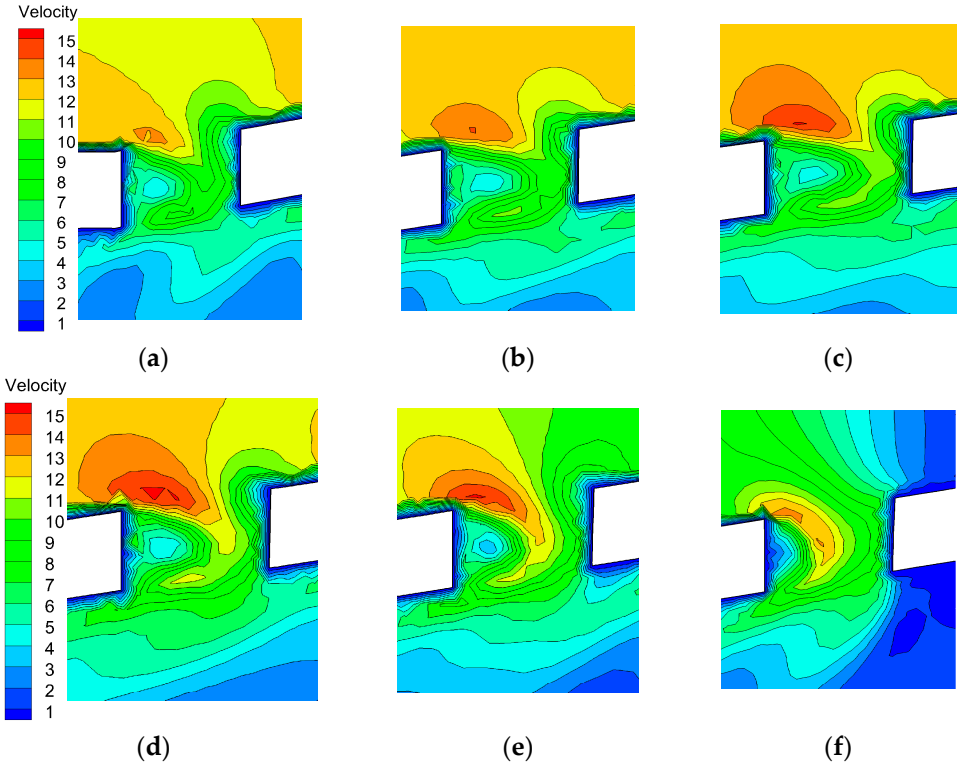

Figure 9. Velocity distribution diagram in cleaning slot. (**a**) Slot 1 (**b**) Slot 2 (**c**) Slot 3 (**d**) Slot 4 (**e**) Slot 5 (**f**) Slot 6. The first row from left to right represents slots 1 to 3, while the second row from left to right represents slots 4 to 6.

The velocity cloud image on the section of the cleaning separation core was extracted, as shown in Figure 9. The lower part in the figure is the outer side of the cleaning separation core, and the upper part is the inner side of the cleaning separation core. In the same cleaning slot, the internal angular velocity of the upstream skeleton is high, while the internal angular velocity of the downstream skeleton is low. Vortex is generated in each cleaning slot, and the vortices are located near the upstream skeleton. The penetration velocity and shear velocity in the slot are shown in Table 5.

Table 5. Penetration velocity and shear velocity.

Slot Number	1	2	3	4	5	6
Average penetration velocity/(m·s^{-1})	3.63	3.89	4.23	4.47	4.89	4.72
Average shear velocity/(m·s^{-1})	3.42	3.64	4.12	4.63	5.64	5.27
Average shear velocity on area B/(m·s^{-1})	3.74	3.75	4.35	4.78	5.81	5.34

From slot 1 to slot 6, the average penetration velocity first increases and then decreases. In slot 5, the penetration velocity is highest, and the average shear velocity also shows the same phenomenon. In slot 6, the penetration velocity and shear velocity decrease because slot 6 is located at the tail end of the cleaning separation core, with a lower mainstream velocity. The incoming airflow gradually approaches the vortex, reducing the vortex area and causing a decrease in the skeleton shear flow velocity. The shear flow velocity in area B is higher than the average shear flow velocity, indicating a stronger cleaning ability near area B, consistent with the analysis above. The distribution range of average shear flow velocity in the slot is 3.42–5.64 m/s, indicates that the structure design of the cleaning separation core is reasonable and can form vortices in the slot. The characteristic parameters of the vortices can meet the requirements of blockage removal.

5.3. Particle Movement Analysis

To further analyze the actual cleaning effect of vortices in the slot, CFD-DEM coupling simulation was conducted, and the air intake speed was set to 11.5 m/s. The process of vortex blockage removal can be divided into three stages. In the first stage, a large amount of mixture enters the cleaning separation core under the action of the airflow, collides with the downstream skeleton under the action of the airflow, and enters the cleaning slot. In the second stage, when the mixture in the slot collides with the sieve, the ratooning rice is sieved out through the sieve, while impurities remain on the sieve. In the third stage, impurities continuously move towards the upstream skeleton under the action of shear flow. After moving to the upstream skeleton, some impurities remain at the upstream skeleton, while others continue to move with the vortex. During the cleaning process, vortices can effectively remove blockages. Comparing the scatter plots of particle motion trajectories in slots 1, 3, and 5, the sampling time is the 4th second. The zero point on the coordinate axis in the figure represents the inner corner point of the upstream skeleton of the cleaning slot, the unit of the coordinate axis is mm (Figure 10).

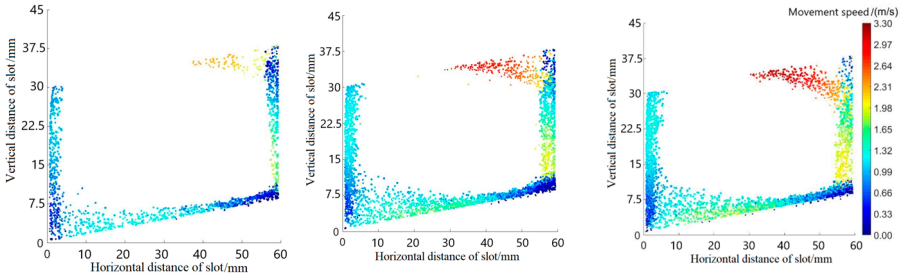

(**a**) slot 1 (**b**) slot 3 (**c**) slot 5

Figure 10. Scatter plots of particle motion trajectories in slots 1, 3, and 5.

As shown in the Figure 10, the shear flow on the upstream skeleton is mainly laminar flow with lower average velocity and smaller velocity gradient, while the shear flow on the downstream skeleton is mainly turbulent flow with higher velocity and larger velocity gradient. The higher the velocity of shear flow, the greater the velocity gradient, the greater the particle movement speed, and the more obvious the Brownian motion of particles. Therefore, the closer the cleaning slot is to the end of the cleaning separation core, the more dispersed the trajectory of particle flow on its wall surface.

Count the number of particles on the three positions of the sieve, as shown in Table 6. The number of particles on the surface of the sieve increases continuously from slot 1 to slot 6. This is caused by the spiral discharge of impurities. The impurities on the sieve are continuously spiraling under the action of the main airflow. When the impurities reach slot 6, the quantity of impurities reaches its maximum. The proportion of impurity particles on the overflow sieve is between 9.8% and 13.4%, which is significantly lower than that of the front sieve and the rear sieve. The phenomenon indicates that the vortex has a strong ability to clear blockages on the sieve.

Table 6. The number of impurity particles captured in each slot.

Slot Number		1	2	3	4	5	6
The number of captured particles		1475	1530	1578	1649	1790	1847
front sieve	Number	480	549	610	575	513	362
	Ratio/%	32.5	35.9	38.7	34.7	28.7	19.6
overflow sieve	Number	196	188	171	162	234	247
	Ratio/%	13.3	12.3	10.8	9.8	13.1	13.4
rear sieve	Number	799	793	797	908	1025	1238
	Ratio/%	54.2	51.8	50.5	55.1	57.3	67.0

6. Bench Test

6.1. Test Method

To verify the actual cleaning effect of vortices in the slot, bench tests were conducted at the Lei Si Building of the School of Agricultural Engineering, Jiangsu University. The comparison group used a traditional harvester cleaning system, and after the experiment, the grain impurity rate, grain loss rate, and sieve blockage rate were compared. Before conducting the bench test, place a collection bag under the threshing drum of the ratooning rice harvester to collect the mixed material. During the experiment, the mixture material was manually fed at a speed of 3.0 kg/s, with a total feed mass of 30 kg and a moisture content of 29.48%. The wind speed at the outlet of the fan is set to 12 m/s, and the wind speed measurement is carried out using the AS-H8 high-precision anemometer produced by Avos, as shown in Figure 11 (Please refer to the Supplementary Materials).

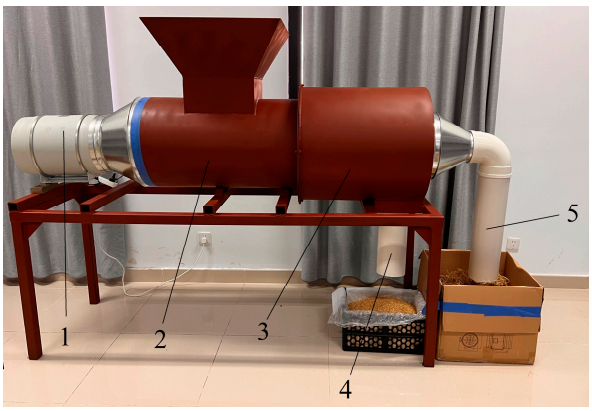

Figure 11. Cleaning bench test. (1) Fan (2) Transportation pipe (3) Cleaning room (4) Clean grain discharge pipe (5) Waste discharge pipe.

Selecting the grain impurity rate Y_1, grain loss rate Y_2, and sieve blockage rate Y_3 as experimental indicators, the quick calculation formula is as follows:

$$\begin{cases} Y_1 = \frac{m_k}{m_k+m_i} \times 100\% \\ Y_2 = \frac{m_l}{m_r} \times 100\% \\ Y_3 = \frac{m_c}{m_h+\mathrm{m}_r} \times 100\% \end{cases} \quad (12)$$

where Y_1, Y_2 and Y_3 are the grain impurity rate and grain loss rate and sieve blockage rate, respectively, %; m_k is the mass of impurities in the clean grain collection box, g; m_i is the mass of ratooning rice in the clean grain collection box, g; m_l is the mass of ratooning rice in the miscellaneous residue collection box, g; m_r is the total mass of ratooning rice fed, g; m_c is the mass of blockage on the cleaning separation core, g; m_h is the total mass of feed impurities, g.

6.2. Result Analysis

Weigh the rice grains cleaned by the spiral step cleaning device and the traditional cleaning device respectively, calculate the grain impurity rate, grain loss rate, and sieve blockage rate [8]. The experimental results are shown in Figure 12 and Table 7. As shown in the Figure 12, there is still a lot of impurities mixed in the ratooning rice after cleaning with traditional cleaning devices, while the purity of the grains is higher after cleaning with spiral step cleaning devices.

(**a**) (**b**)

Figure 12. Comparison of cleaning effect. (**a**) Traditional cleaning device (**b**) Spiral step cleaning device.

Table 7. Bench test results.

Index	Grain Impurity Rate/%	Grain Loss Rate/%	Sieve Blockage Rate/%
Spiral step cleaning device	1.35	2.13	0.09
Traditional cleaning equipment	2.55	3.47	90
Simulation result	1.23	2.05	0.02

After three experiments and calculating the average value, the spiral step cleaning device showed an average grain impurity rate of 1.35%, an average grain loss rate of 2.13%, and an average sieve blockage rate of $\leq$0.1% after cleaning. The bench test was consistent with the numerical simulation phenomenon, indicating that the numerical simulation results are reliable. The experimental results show that the vortex generated by the spiral step cleaning device can effectively reduce the blockage of the sieve.

7. Discussion and Perspectives

Step cleaning is a research on the feeding process of filter feeding fish. Currently, the application of step cleaning principle mainly focuses on the collection of algae and small organisms [26], and there has been no application in grain cleaning technology. The step cleaning technology can utilize the shear flow on the surface of the sieve to remove blockages, effectively improving the performance of the cleaning device and addressing the shortcomings of traditional cleaning systems.

Although the structure of the cleaning slot of the step cleaning device may seem simple, there are still many parameters that can be adjusted, such as cone angle, slot height, slot width, and spiral rise angle. When one of the geometric parameters changes, the other parameters will also change accordingly. The ratio of the inlet area of the mixture to the screen area is a key parameter to ensure the formation of vortices in the cleaning slot, and its value should usually be greater than 1 [37]. In this design, the ratio of the mixture inlet

area to the screen area of the spiral step cleaning device is 1.32, so the vortex in the slot can meet the conditions for clearing blockages. In traditional cleaning device design, increasing the length of the equipment can effectively improve cleaning efficiency. However, in step cleaning, simply increasing the length of the device will not significantly improve cleaning efficiency, and may even reduce the cleaning effect of vortices.

Optimizing the structure of the step spiral skeleton can increase the cleaning area of the sieve, thereby improving the cleaning ability of the device. Therefore, in the next step of research, a multi factor experimental method should be used to obtain the optimal structural parameter combination of the spiral step cleaning device. By optimizing the structural parameters of the device, the cleaning efficiency and vortex blockage removal effect can be maximized.

8. Conclusions

- In response to the problems of high grain impurity rate and grain loss rate in the cleaning of ratooning rice using ordinary cleaning devices, a spiral step cleaning device was designed by integrating mechanical and pneumatic combination separation technology, which can break the force balance of blockages at the sieve hole. The key structural parameters of the cleaning device and the wind speed of the fan have been determined.
- Simulation analysis was conducted on the flow state inside the cleaning device, and the results showed that along the direction of airflow movement, the average penetration velocity and average shear velocity both showed a trend of first increasing and then decreasing. The penetration velocity and shear velocity were highest in slot 5, and vortices were generated in each slot, which can meet the requirements for sieve cleaning.
- An analysis was conducted on the particle motion under the action of vortices, and the results showed that the proportion of impurities on the middle sieve was between 9.8% and 13.4%, which was significantly lower than that on the front and rear sieves. The impurities did not accumulate on the middle sieve, and the effect of vortex blockage was in line with expectations. The results of the bench test and simulation test are consistent, indicating that it is feasible to use a spiral step cleaning device to clean ratooning rice. The vortices in the slot can remove blockages on the sieve. This study provides a foundation for the subsequent research of the spiral step cleaning device.

Supplementary Materials: The following are available online at https://www.mdpi.com/article/10.3390/agriculture14060866/s1, Video S1: title: Vortex Cleaning De-vice for Rice Harvester.

Author Contributions: Conceptualization, X.C.; methodology, W.L.; software, S.Z.; validation, W.L. and S.Z.; formal analysis, S.Z.; investigation, W.L.; resources, W.L.; data curation, W.L.; writing—original draft preparation, W.L.; writing—review and editing, S.Z. and X.C.; visualization, S.Z.; supervision, S.Z.; project administration, X.C.; funding acquisition, X.C. All authors have read and agreed to the published version of the manuscript.

Funding: This research was funded by the Key Core Technology Research Project of the Ministry of Agriculture and Rural Affairs on Agricultural Production: Light and Simple Grain Combine Harvester (NK2022160401) and Jiangsu Funding Program for Excellent Postdoctoral Talent.

Institutional Review Board Statement: Not applicable.

Data Availability Statement: The data that support the findings of this study are available on request from the corresponding author.

Acknowledgments: The authors gratefully acknowledge the editors and anonymous reviewers for their constructive comments on our manuscript. The authors would like to express their gratitude to EditSprings (https://www.editsprings.cn) (accessed on 1 April 2024.) for the expert linguistic services provided.

Conflicts of Interest: The authors declare no conflict of interest.

References

1. Zhao, Z.; Huang, H.; Yin, J.; Yang, S.X. Dynamic analysis and reliability design of round baler feeding device for rice straw harvest. *Biosyst. Eng.* **2018**, *174*, 10–19. [CrossRef]
2. Wang, Q.; Mao, H.; Li, Q. Modelling and simulation of the grain threshing process based on the discrete element method. *Comput. Electron. Agric.* **2020**, *178*, 105790. [CrossRef]
3. Liu, W.; Luo, X.; Zeng, S.; Zang, Y.; Wen, Z.; Zeng, L.; Gu, W. Numerical simulation and experiment of grain motion in the conveying system of ratooning rice harvesting machine. *Int. J. Agric. Biol. Eng.* **2022**, *15*, 103–115. [CrossRef]
4. Liu, W.; Luo, X.; Zeng, S. The Design and Test of the Chassis of a Triangular Crawler-Type Ratooning Rice Harvester. *Agriculture* **2022**, *12*, 890. [CrossRef]
5. Liu, W.; Luo, X.; Zeng, S. Performance test and analysis of the self-adaptive profiling header for ratooning rice based on fuzzy PID control. *Trans. Chin. Soc. Agric. Eng.* **2022**, *38*, 1–9.
6. Wang, H.; Li, Y.; Xu, L. Simulation and experiment of air flow field in the cleaning device of ratooning rice combine harvesters. *Chin. Soc. Agric. Eng.* **2020**, *36*, 84–92.
7. Xu, L.; Li, Y.; Li, Y. Research Progress on Cleaning Technology and Device of Grain Combine Harvester. *Trans. Chin. Soc. Agric. Mach.* **2019**, *50*, 1–16.
8. Leng, J.; Li, X.; Du, Y. Analysis and optimization of internal flow field of cleaning device of single longtitudinal axial flow grain combine harvester. *Chin. Soc. Agric. Eng.* **2020**, *36*, 39–48.
9. Soldinger, M. Transtant velocity of a crushed rock material bed on a screen. *Miner. Eng.* **2002**, *15*, 7–17. [CrossRef]
10. Zhu, Y.; Ma, Z.; Chen, S.; Souleymane, N.; Li, Y.; Jiang, S. Study on BPNN prediction of variable amplitude anti-blocking screening performance: Based on EDEM-RecurDyn simulation. *J. Chin. Agriculation Mech.* **2022**, *43*, 75–80.
11. Yang, H.; Ma, H. Test on the application of polyurethane elastomer screen deck in circular vibrating screen. *Met. Mine* **2003**, *01*, 51–53.
12. Li, Y.; Ma, Z.; Xu, L. Tribological characteristics of adhesive materials on cleaning sieve of rape combine harvester. *Trans. Chin. Soc. Agric. Mach.* **2010**, *41*, 54–57.
13. Brooks, H.; Haines, G.E.; Lin, M.C.; Sanderson, S.L. Physical modeling of vortical cross-step flow in the American paddlefish, *Polyodon spathula*. *PLoS ONE* **2018**, *13*, e0193874. [CrossRef] [PubMed]
14. Cheer, A.; Cheung, S.; Hung, T.-C.; Piedrahita, R.H.; Sanderson, S.L. Computational fluid dynamics of fish gill rakers during crossflow filtration. *Bull. Math. Biol.* **2012**, *74*, 981–1000. [CrossRef] [PubMed]
15. Gorb, Y.; Mierka, O.; Rivkind, L.; Kuzmin, D. Finite element simulation of three-dimensional particulate flows using mixture models. *J. Comput. Appl. Math.* **2014**, *270*, 443–450. [CrossRef]
16. Ismail, N.I.; Kuang, S.; Tang, Y.; Yu, A. CFD-DEM evaluation of screen types for sand control applications. *Powder Technol.* **2022**, *404*, 117496. [CrossRef]
17. Qian, F.; Huang, N.; Lu, J.; Han, Y. CFD-DEM simulation of the filtration performance for fibrous media based on the mimic structure. *Comput. Chem. Eng.* **2014**, *71*, 478–488. [CrossRef]
18. Stel, H.; Franco, A.T.; Junqueira, S.L.M.; Erthal, R.H.; Mendes, R.; Gonçalves, M.A.L.; Morales, R.E.M. Turbulent flow in d-type corrugated pipes: Flow pattern and friction factor. *J. Fluids Eng.* **2012**, *134*, 121202. [CrossRef]
19. Liu, C.; Chung, T. Forced convective heat transfer overskeletons at various separation. *Int. J. Heat Mass Transf.* **2012**, *55*, 5111–5119. [CrossRef]
20. Schroeder, A.; Marshall, L.; Trease, B. Development of helical, fish-inspired spiral step cleaning device for collecting harmful algae. *Bioinspir. Biomim.* **2019**, *14*, 056008. [CrossRef] [PubMed]
21. Dou, Y.; Tian, D.; Sun, Z.; Liu, Q.; Zhang, N.; Kim, J.H.; Jiang, L.; Dou, S.X. Fish gill inspired crossflow for efficient and continuous collection of spilled oil. *ACS Nano* **2017**, *11*, 2477–2485. [CrossRef] [PubMed]
22. Liu, C.; Wang, Y.; Yang, Y.; Duan, Z. New omega vortex identification method. *Sci. China Phys. Mech. Astron.* **2016**, *59*, 684711. [CrossRef]
23. Zhu, H.; Zhou, Z.; Yang, R.; Yu, A. Discrete particle simulation of particulate systems: Theoretical developments. *Chem. Eng. Sci.* **2007**, *62*, 3378–3396. [CrossRef]
24. Chu, K.; Wang, B.; Yu, A.; Vince, A. Modelling the multiphase flow in dense medium cyclones. *J. Comput. Multiph. Flows* **2010**, *2*, 249–272. [CrossRef]
25. Johnson, K.L.; Kendall, K.; Roberts, A.D. Surface energy and the contact of elastic solids. Proceedings of the royal society of London. A. mathematical and physical sciences. *Proc. R. Soc. A Math. Phys. Eng. Sci.* **1971**, *324*, 301–313.
26. Smith, J.C.; Sanderson, S.L. Particle retention in suspension-feeding fish after removal of filtration structures. *Zoology* **2013**, *116*, 348–355. [CrossRef]
27. Xu, Z.; Mao, X.; Gu, Y.; Chen, X.; Kuang, W.; Wang, R.; Shao, X. Analysis of hydrodynamic filtration performance in a cross-step filter for drip irrigation based on the cfddem coupling method. *Biosyst. Eng.* **2023**, *232*, 114–128. [CrossRef]
28. Duran-Ros, M.; Puig-Bargués, J.; Arbat, G.; Barragán, J.; de Cartagena, F.R. Definition of a SCADA system for a microirrigation network with effluents. *Comput. Electron. Agric.* **2008**, *64*, 338–342. [CrossRef]
29. Zhu, D.; Wang, R.; Ruan, H. Response of process of Y-net filter clogging to organic fertilizer concentration. *Trans. Chin. Soc. Agric. Mach.* **2020**, *51*, 332–337.

30. Krzysztof, L.; Krzysztof, J. The Quality of Winter Wheat Grain by Different Sowing Strategies and Nitrogen Fertilizer Rates: A Case Study in Northeastern Poland. *Agriculture* **2024**, *14*, 552.
31. Twizerimana, A.; Niyigaba, E.; Mugenzi, I.; Ngnadong, W.A.; Li, C.; Hao, T.Q.; Shio, B.J.; Hai, J.B. The combined effect of different sowing methods and seed rates on the quality features and yield of winter wheat. *Agriculture* **2020**, *10*, 153. [CrossRef]
32. Souza, E.; Martin, J.; Guttieri, M.; O'Brien, K.; Habernicht, D.; Lanning, S.; McLean, R.; Carlson, G.; Talbert, L. Influence of genotype, environment, and nitrogen management on spring wheat quality. *Crop Sci.* **2004**, *44*, 425–432. [CrossRef]
33. Li, H.; Li, Y.; Tang, Z.; Xu, L.; Zhao, Z. Numerical simulation and analysis of vibration screening based on EDEM. *Trans. Chin. Soc. Agric. Eng.* **2011**, *27*, 117–121.
34. Xu, L.; Li, Y. Critical speed of impact damage on a rice kernel. *Trans. Chin. Soc. Agric. Mach.* **2009**, *40*, 54–57.
35. Xu, J.; Sun, S.; Li, X.; Zeng, Z.; Han, C.; Tang, T.; Wu, W. Research on the Population Flow and Mixing Characteristics of Pelleted Vegetable Seeds Based on the Bonded-Particle Model. *Agriculture* **2024**, *14*, 752. [CrossRef]
36. Qi, J.; Gao, J.; Chen, S.; Chen, W.; Yang, L.; Meng, H.; Kan, Z. Parameter Optimization of a Conveying and Separating Device Based on a Five-Stage Screw and Vibrating Screen for Tiger Nut Harvesters. *Agriculture* **2024**, *14*, 682. [CrossRef]
37. Sanderson, S.L.; Roberts, E.; Lineburg, J.; Brooks, H. Fish mouths as engineering structures for vortical cross-step filtration. *Nat. Commun.* **2016**, *7*, 11092. [CrossRef] [PubMed]

Disclaimer/Publisher's Note: The statements, opinions and data contained in all publications are solely those of the individual author(s) and contributor(s) and not of MDPI and/or the editor(s). MDPI and/or the editor(s) disclaim responsibility for any injury to people or property resulting from any ideas, methods, instructions or products referred to in the content.